Natural Rubber/Poly(ethylene-*co*-vinyl acetate)-Blend-Based Nanocomposites

Jamaliah Sharif,[1] Wan Md Zin Wan Yunus,[1] Khairulzaman Hj Dahlan,[2] Mansor Hj Ahmad[1]

[1]*Chemistry Department, Faculty of Science and Environmental Studies, Universiti Putra Malaysia, 43400 UPM Serdang, Selangor, Malaysia*
[2]*Malaysian Institute for Nuclear Technology Research, Bangi, 43000 Kajang, Malaysia*

Received 9 November 2004; accepted 15 June 2005
DOI 10.1002/app.23121
Published online in Wiley InterScience (www.interscience.wiley.com).

ABSTRACT: Natural rubber (NR)/poly(ethylene-*co*-vinyl acetate) (EVA) blend–clay nanocomposites were prepared and characterized. The blend nanocomposites were prepared through the melt mixing of NR/EVA in a ratio of 40/60 with various amounts of organoclay with an internal mixer followed by compression molding. X-ray diffraction patterns revealed that the nanocomposites formed were intercalated. The formation of the intercalated nanocomposites was also indicated by transmission electron microscopy. Scanning electron microscopy, used to study the fractured surface morphology, showed that the distribution of the organoclay in the polymer matrix was homogeneous. The tensile modulus of the nanocomposites increased with an increase in the organoclay content. However, an increase in the organoclay content up to 5 phr did not affect the tensile strength, but the organoclay reduced this property when it was increased further. This study also indicated that a low silicate content dispersed in the blend matrix was capable of increasing the storage modulus of the material. The addition of the organoclay also increased the decomposition temperature of the NR/EVA blends. © 2006 Wiley Periodicals, Inc. J Appl Polym Sci 100: 353–362, 2006

Key words: blends; clay; nanocomposites; rubber

INTRODUCTION

Polymer/clay nanocomposites are a new class of materials that show improved properties at very low clay loadings in comparison with those of conventional composites. Among the improved properties are mechanical, dimensional, and thermal stability, flame retardancy, and permeability.[1] To obtain good interfacial adhesion and mechanical properties, the hydrophilic clay needs to be modified before its introduction into most polymer matrices, which are usually organophilic. The clay modification is commonly achieved by ion-exchange reactions of sodium ions by organophilic cations such as alkyl ammonium or alkyl phosphonium.[2,3] Many polymer systems have been investigated since the possibility of melt mixing polymers with an organoclay to produce nanocomposites was reported by Vaia et al.[4] The work was expanded with various polymers, and these include poly(ethylene-*co*-vinyl acetate) (EVA)[5–7] and natural rubber (NR).[8,9]

Preparations of nanocomposites with a single polymer matrix are becoming common nowadays. However, the preparation of nanocomposites based on blends seems to be new in nanocomposites studies. Chow et al.[10] reported their findings on the compatibilizing effect of maleated polypropylene on the mechanical properties and morphology of injection-molded polyamide 6/polypropylene/organoclay nanocomposites.

In this article, we describe our attempt to prepare NR/EVA-blend-based clay nanocomposites and study their properties. NR/EVA blends are very attractive because of the excellent properties of both constituents. It has been reported that the addition of NR to EVA increases the melt elasticity of the system.[11] In addition, the presence of EVA in high proportions increases the thermal aging resistance of NR/EVA blends.[12]

EXPERIMENTAL

Materials

NR (SMRL-grade) was purchased from Guthrie Corp. (M) Bhd. (Malaysia). EVA (Polene EVA copolymer), containing less than 18 wt % vinyl acetate, with a melt flow index of 2.4 g/10 min (at 190°C and 2.16-kg load) and with a density of 0.938 g/cc, was bought from Thailand Petrochemical. Sodium montmorillonite (Na-MMT; Kunipia F) with a cation-exchange capacity of 119 mequiv/100 g was purchased from Kunimine Industries Co. (Japan). Dimethyl dihydrogenated tal-

Correspondence to: J. Sharif (jamaliah@mint.gov.my).
Contract grant sponsor: Ministry of Science of Malaysia (through an IRPA grant).

low ammonium modified montmorillonite [Cloisite 20A (C20A)] was bought from Southern Clay Products, Inc. (United States). Dodecyl amine was supplied by Merck (Germany). Hydrochloric acid was purchased from BDH (England).

Modification of the clay

Organoclay was prepared by a cation-exchange process in an aqueous solution by the vigorous stirring of 20 g of Na-MMT dispersed in 800 mL of distilled water at 80°C with 50 mmol of dodecyl ammonium chloride dissolved in 200 mL of 0.25*M* HCl for 1 h. The precipitate was then filtered and washed with hot distilled water until it free of chloride ions (detected by a 1*N* $AgNO_3$ solution). It was then dried in a vacuum oven at 60°C for 24 h. The dry organophilic montmorillonite was ground, and the particles less than 75 μm in size were used for the preparation of the nanocomposites. The product was labeled DDA-MMT.

Nanocomposite preparation

In this work, an NR/EVA blend with a ratio of 40/60 (w/w) was used for the preparation of blend-based nanocomposites. The EVA pellet (ca. 27 g) was first mixed with an internal mixer (Haake) at a temperature of 125°C and a rotor speed of 50 rpm for 1 min. NR (17.8 g) was then added to the mixer and allowed to mix with EVA for 2 min. Immediately after the mixing period was complete, the required amount of DDA-MMT was added to the mixer, and the mixing was continued for 7 min. The obtained composites were then preheated at 125°C, hot-pressed at 125°C and 110 kg/cm^2, and cold-pressed for 4 min to obtain slabs ($150 \times 150 \times 1$ mm^3 and $130 \times 130 \times 3$ mm^3).

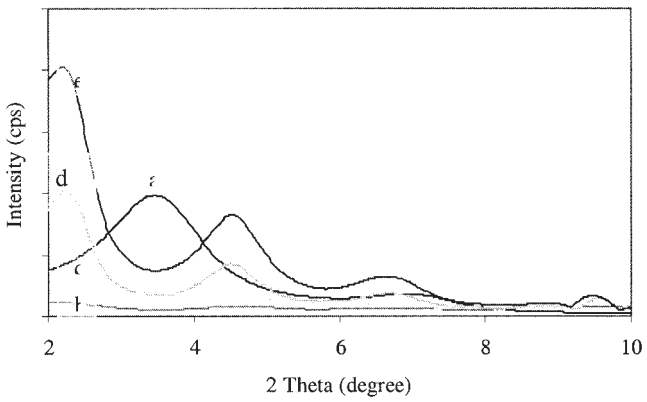

Figure 2 XRD patterns of (a) C20A, (b) NR/EVA/1C20A, (c) NR/EVA/3C20A, (d) NR/EVA/5C20A, and (e) NR/EVA/10C20A.

Characterization

X-ray diffraction (XRD) was performed at room temperature with a Shimadzu XRD 600 X-ray diffractometer. The X-ray beam was nickel-filtered Cu Kα (wavelength = 1.542 Å) radiation operated at 30 kV and 30 mA. Data were obtained for a 2θ range of 2–10° at a rate of 1°C/min.

The surface morphology of the nanocomposite samples was observed with a FEI Quanta 400 scanning electron microscope operated at 25 kV. The cryogenically fractured samples were soaked with toluene for 24 h and then dried in an oven for 24 h. The dried samples were coated with gold with a Bio-Rad coating system. The scanning electron microscopy (SEM) photographs were recorded at a magnification of 20,000×.

Clay distribution in the nanocomposites was studied with a Leo 912AB energy-filter transmission electron microscope with an acceleration voltage of 120 keV. The samples were prepared with a Reichert Jung

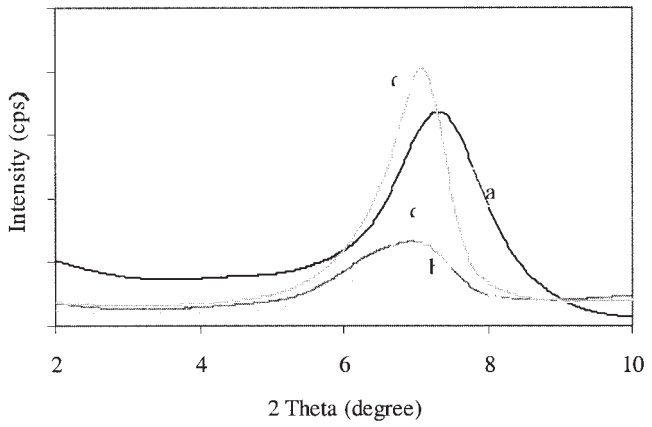

Figure 1 XRD patterns of (a) Na-MMT, (b) NR/EVA/3Na-MMT, (c) NR/EVA/5Na-MMT, and (d) NR/EVA/10Na-MMT.

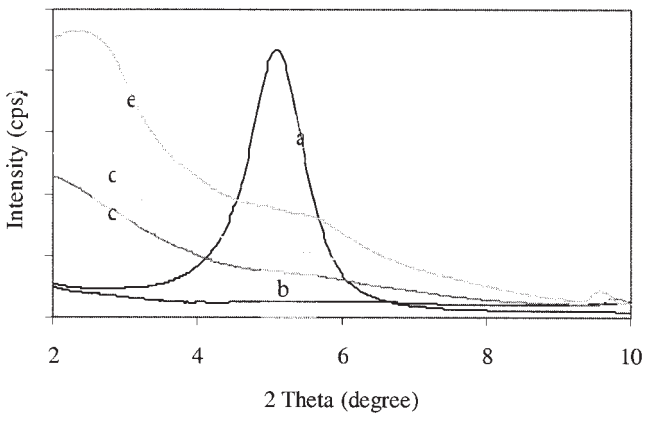

Figure 3 XRD patterns of (a) DDA-MMT, (b) NR/EVA/1DDA-MMT, (c) NR/EVA/3DDA-MMT, (d) NR/EVA/5DDA-MMT, and (e) NR/EVA/10DDA-MMT.

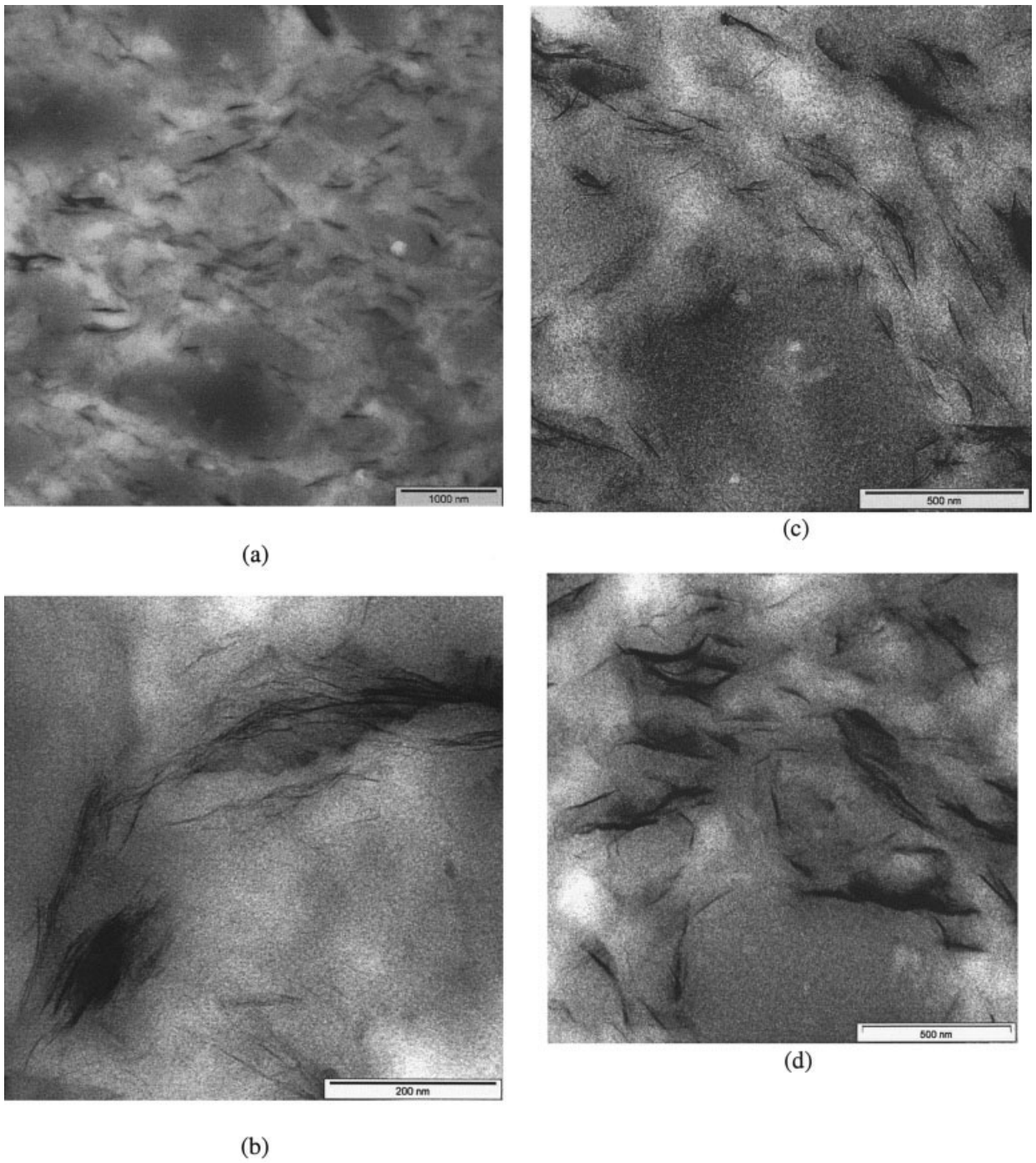

Figure 4 TEM pictures of (a) NR/EVA/3DDA-MMT (1000 nm), (b) NR/EVA/3DDA-MMT (200 nm), (c) NR/EVA/3DDA-MMT (500 nm), and (d) NR/EVA/3C20A (500 nm).

Ultracut E microtome equipped with a cryosectioning unit. Thin sections of about 90 nm were cut with a diamond knife cooled at −120°C.

Tensile tests were carried out according to ASTM D 417 with an Instron model 4301 testing machine. The dumbbell-shaped specimens were extended at a crosshead speed of 100 mm/min. The reported values of the tensile properties represent averages of the results from test runs on five specimens. The standard deviations were 2–5% for the tensile strength, about 3% for the modulus at 300% extension, and 5% for the elongation at break.

The dynamic mechanical analysis of the nanocomposites was carried out with a PerkinElmer 7E dynamic mechanical analyzer with a three-point-bending fixture. Rectangular samples ($12.6 \times 5 \times 1$ mm^3) were used in the study, and the analysis was carried out from −140 to 200°C at a heating rate of 5°C/min

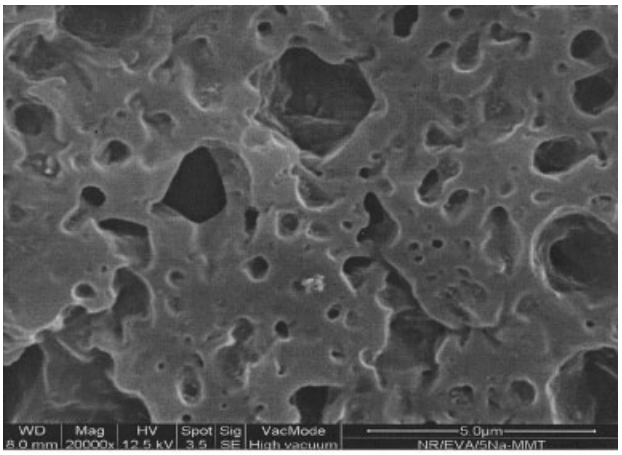

(a)

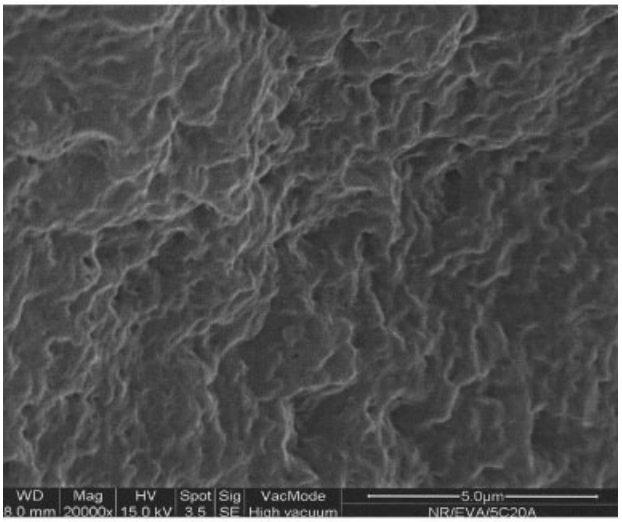

(b)

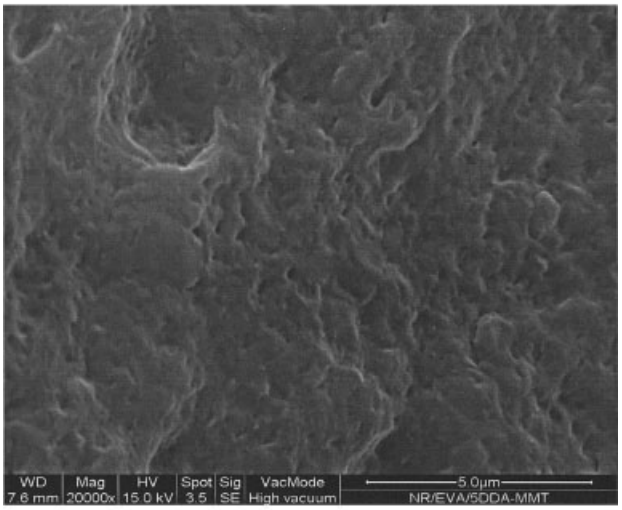

(c)

Figure 5 SEM micrographs showing the fractured surfaces of (a) NR/EVA/Na-MMT, (b) NR/EVA/C20A, and (c) NR/EVA/DDA-MMT.

and a frequency of 1 Hz. The amplitude and tension were fixed at 10 μm and 110%, respectively.

The thermogravimetry of the samples was studied with a PerkinElmer TGA7. Thermograms of approximately 10-mg samples were recorded from 50 to 700°C at a heating rate of 10°C/min under a dynamic nitrogen atmosphere.

RESULTS AND DISCUSSION

XRD study

Figure 1 shows the XRD patterns of Na-MMT and NR/EVA/Na-MMT composites with various concentrations of the unmodified clay in the 2θ range of 2–10°. The 001 peak of Na-MMT is at $2\theta = 7.28°$, corresponding to an interlayer distance of 12.13 Å. This peak is shifted to 2θ values of 6.70, 6.86, 6.99, and 6.99°, corresponding to interlayer distances of 13.31, 13.07, 12.63, and 12.63 Å for NR/EVA/clay composites containing 1, 3, 5, and 10 phr Na-MMT, respectively. As expected, the hydrophilic nature of Na-MMT is hardly intercalated by the NR and EVA molecular chains. The unmodified Na-MMT particles are simply incorporated into the SMRL matrix in an agglomerated state.

The XRD patterns of C20A and NR/EVA/C20A nanocomposites are shown in Figure 2. The XRD patterns show that the 001 peak of C20A is at $2\theta = 3.60°$, corresponding to an interlayer distance of 24.51 Å. Nanocomposites containing 1, 3, 5, and 10 phr C20A show the 001 peak at 2θ values of 2.41, 2.42, 2.33, and 2.34°, respectively, corresponding to interlayer distances of 36.63, 36.44, 37.93, and 37.79 Å, respectively. The increase in the interlayer distance of C20A from 24.51 to 36.63, 36.44, 37.93, and 37.79 Å in the NR/EVA/C20A nanocomposites containing 1, 3, 5, and 10 phr organoclay, respectively, indicates that intercalation of the polymer chains into the clay interlayers has occurred. The diffraction patterns of the 001 plane indicate that the clay layers are at least partially arranged into aggregates that comprise regularly spaced layers.[13]

Figure 3 displays the XRD patterns of DDA-MMT and NR/EVA/DDA-MMT nanocomposites. DDA-MMT shows a sharp peak at $2\theta = 5.26°$, which is equivalent to an interlayer distance of 16.71 Å. For nanocomposites containing 3, 5, and 10 phr DDA-MMT, the diffraction peak is shifted to lower 2θ angles at 2.31, 2.42, and 2.65°, which indicate that the interlayer distances increase to 38.21, 36.50, and 33.31 Å, respectively. The increase in the interlayer distance indicates the formation of intercalated nanocomposites. However, there is no diffraction peak for the nanocomposite containing 1 phr DDA-MMT. The absence of the diffraction peak is probably due to the fact that either the clay concentration in the nanocompos-

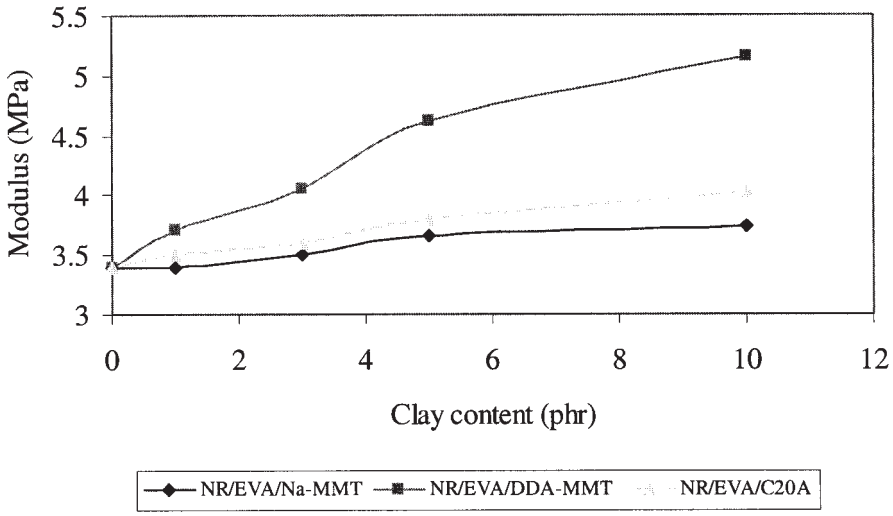

Figure 6 Modulus at 300% elongation of NR/EVA/clay composites.

ite is too low or an exfoliated nanocomposite has formed. This can be further confirmed with transmission electron microscopy (TEM) observation.

In the clay modified by the cation-exchange process, the surfactant molecules are intercalated between the layers of the silicate through a cation-exchange reaction and enlarge the distance between the silicate layers, decrease the clay hydrophilic properties, and enhance its compatibility with the polymer. With the help of mechanical shear during the melt-mixing process with a Haake internal mixer, the polymer chains diffuse from the bulk polymer melt into the galleries between the silicate layers, forming intercalated nanocomposites.

TEM

Figure 4(a–d) shows TEM images of NR/EVA-blend-based nanocomposites containing 3 phr DDA-MMT (1000, 200, and 500 nm) and 3 phr C20A (500 nm), respectively. The dark lines represent the stacked silicate layers. In the images intercalated, exfoliated, and aggregated organoclay platelets can be found. In addition, the organoclay has a strong tendency to be located in the EVA phase.

SEM

SEM micrographs of cryofractured surfaces of an NR/EVA/Na-MMT composite and NR/EVA/5C20A and NR/EVA/5DDA-MMT nanocomposites are shown in Figure 5(a–c), respectively. NR/EVA/Na-MMT shows coarse holes of various sizes scattered on the surface, whereas for the nanocomposites, the holes are smaller and shallower. The holes on the surface of NR/EVA/Na-MMT indicate the incompatibility of hydrophilic Na-MMT with the hydrophobic polymer

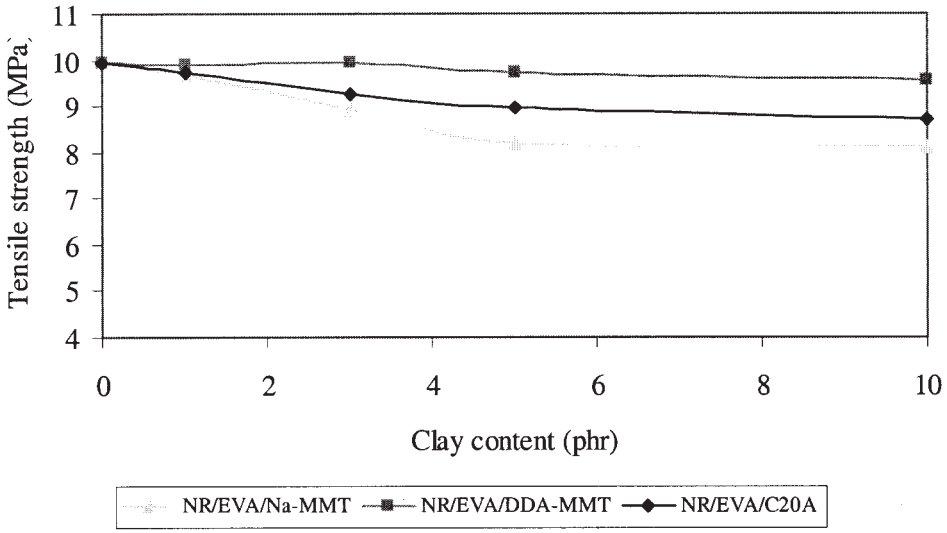

Figure 7 Tensile strength of NR/EVA/organoclay nanocomposites.

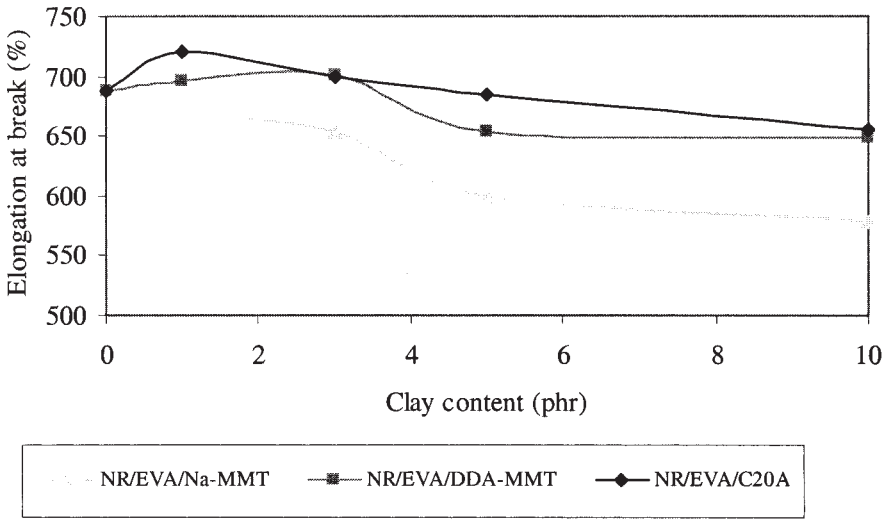

Figure 8 Elongation at break of NR/EVA/organoclay nanocomposites.

matrix. During the soaking process with toluene, NR and EVA that cover the agglomerated clays are dissolved, and the clay particles are washed away, leaving coarse holes on the sample surface. On the other hand, the organoclay, which is distributed homogeneously in the nanocomposites, gives a smoother surface as the clay particles are smaller. This is also indicates the compatibility phenomenon of the organoclay with the polymer matrix, which results in the formation of the nanocomposites.

Tensile properties

Figure 6 shows the modulus at 300% elongation of NR/EVA/Na-MMT composites and NR/EVA/C20A and NR/EVA/DDA-MMT nanocomposites. The modulus of the composites increases with increasing clay content. However, the increase in the modulus of NR/EVA/Na-MMT is smaller than that of the NR/EVA/C20A and NR/EVA/DDA-MMT nanocomposites at all clay concentrations. The poor compatibility between the unmodified clay and the polymer matrix leads to poor distribution of clay [Fig. 5(a)] and hence reduces the stiffness. The addition of a low concentration of organoclay (1–10 phr) increases the tensile modulus of the nanocomposites significantly. For example, the tensile moduli of the C20A and DDA-MMT nanocomposites are 40 and 90% higher than that of the unfilled blend. The increase in the modulus is due to the reinforcement effect by the silicate layers on the polymer matrix. It has been reported that exfoliated silicate layers are the main factor responsible for the stiffness improvement in nanocomposites.[14]

The tensile strength of the composites is shown in Figure 7. The tensile strength of both the NR/EVA/Na-MMT and NR/EVA/C20A composites decreases

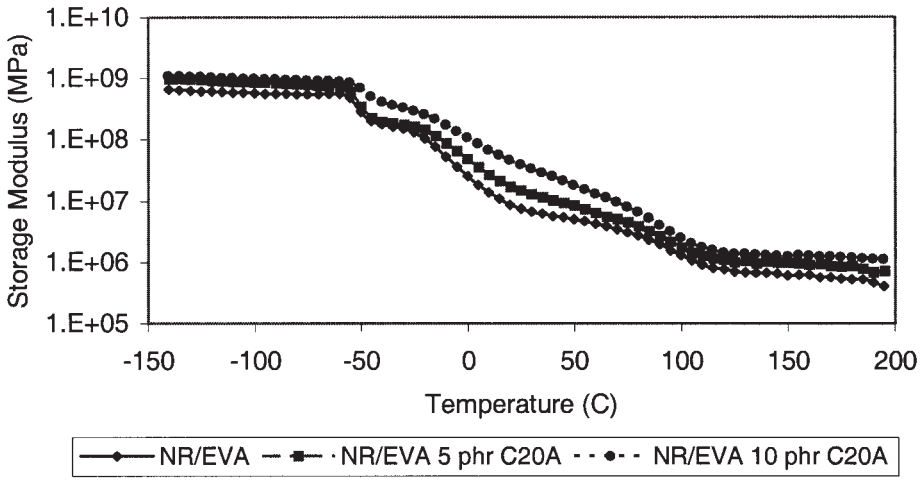

Figure 9 Storage modulus of the NR/EVA blend and its nanocomposites with various concentrations of C20A.

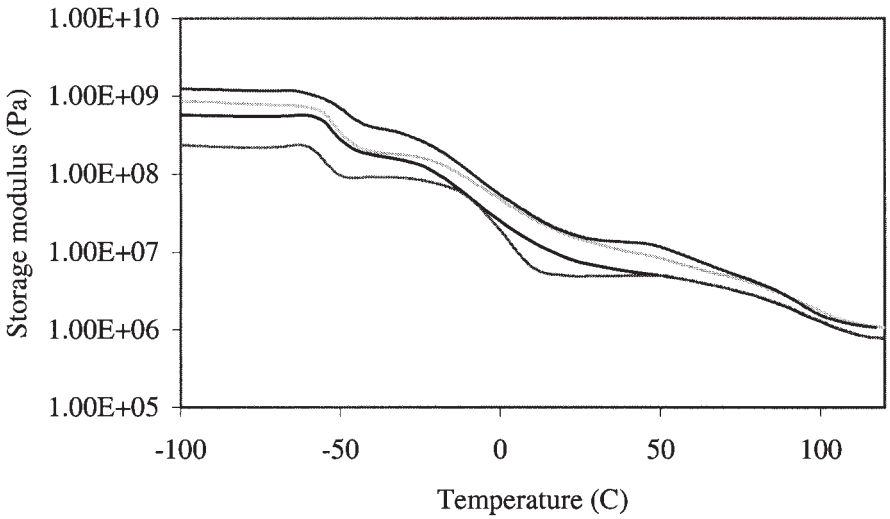

Figure 10 Storage modulus of (a) NR/EVA, (b) NR/EVA/5Na-MMT, (c) NR/EVA/5C20A, and (d) NR/EVA/5DDA-MMT.

with increasing clay concentration. Meanwhile, the tensile strength of the NR/EVA/DDA-MMT nanocomposites remains at about 10 MPa with the clay content up to 5 phr but decreases around 9 MPa when the clay content is increased to 10 phr. The poor reinforcement effect in the nanocomposites is due to the poor dispersion of clay particles. The large size of the clay particles serves as stress concentration and flaws for crack initiation, resulting in premature failure upon uniaxial loading.[15] Similarly, the presence of the organoclay in the NR/EVA matrix does not increase the strength of the compound, even though the formation of intercalated nanocomposites already has been confirmed by the XRD patterns (Figs. 2 and 3). This may be due to the incompatibility of NR and EVA. The poor strength of intercalated nanocomposites was also reported by Noh and Lee[16] for polystyrene (PS)-intercalated nanocomposites, for which they found the ultimate tensile stress of the nanocomposite to be smaller than that of the PS matrix and to decrease with increasing filler content.

The elongation at break of NR/EVA/Na-MMT, NR/EVA/C20A, and NR/EVA/DDA-MMT nanocomposites are presented in Figure 8. Increasing the clay content to 3 phr in the NR/EVA/DDA-MMT nanocomposites increases the elongation at break. However, a further increase in the clay content reduces the elongation. The elongation at break of NR/EVA/C20A also shows an increase in the elongation at break at 1 phr clay and decreases with a further increase in the clay content. On the other hand, the elongation at break of NR/EVA/Na-MMT decreases

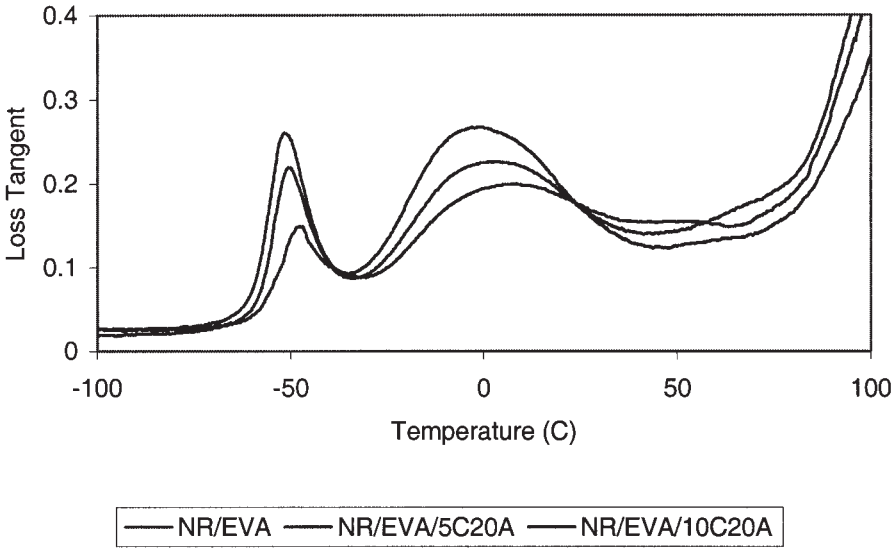

Figure 11 Loss tangent versus the temperature for NR/EVA/clay nanocomposites.

TABLE I
T_g and Area Under the Peak for the NR/EVA Blend Nanocomposites

Sample	T_g of NR (°C)	Area under the curve for NR	T_g of EVA (°C)	Area under the curve for EVA
NR/EVA	−60.0	0.436	−11.1	1.302
NR/EVA5C20A	−58.7	0.343	−8.051	0.929
NR/EVA10C20A	−56.9	0.192	−5.238	0.621

with increasing clay concentration. Such an observation is common in filled polymers, in which the mobility of the polymer chain and shear deformation capability of the polymer are severely reduced in the presence of an inorganic filler.[15]

Dynamic mechanical analysis

The temperature dependence of the storage modulus of NR/EVA/C20A nanocomposites is shown in Figure 9. The storage modulus of the nanocomposites decreases as the temperature increases from −140 to 200°C because of the decrease in the stiffness of the samples at high temperatures. The incorporation of the organoclay into the NR/EVA blends increases the storage modulus. The storage modulus also increases with increasing organoclay content. The results are in agreement with the tensile modulus results measured at 23°C. The storage modulus of the NR/EVA-blend-based nanocomposite containing 10 phr C20A is about 1.2×10^9 Pa, which is 40% higher than that of the unfilled blend. The enhancement of the storage modulus is due to the reinforcement effect of the silicate layers. Figure 10 shows that the storage modulus of NR/EVA/5DDA-MMT is higher than that of the pure NR/EVA blend. In contrast, the NR/EVA/Na-MMT composite has a lower storage modulus than that of the unfilled blend at a temperature below the glass-transition temperature (T_g), but above T_g, the storage modulus is almost the same as that of the unfilled blend, as shown in Figure 10. This is due to the incompatibility between Na-MMT and the NR/EVA blend.

Figure 11 shows the temperature dependence of tan δ of NR/EVA/C20A nanocomposites with 3, 5, and 10 phr clay. The NR/EVA blends exhibit two peaks, which indicate that there are two transitions corresponding to the NR and EVA phases. This clearly indicates the incompatibility of the two components. The incorporation of the organoclay into the NR/EVA blends increases the T_g values of both NR and EVA phases systematically. The T_g values of the nanocomposites obtained from the maximum of tan δ and the areas under the curves are listed in Table I. The shift in T_g can be explained by the dispersion degree of the clay in the nanocomposites. This behavior also can be attributed to the effect of the restriction of the segmental motion of the polymer near the organic–inorganic interface due to the increased adhesion between the polymer and organoclay surface.[17] It is well known that the T_g value of a polymer depends on the mobility of the chain segment of the macromolecules in the polymer matrix. Therefore, if the molecular chain is restricted, movement or relaxation of the chain segment becomes difficult at the original T_g value and becomes easy at higher temperatures.[17] When the NR/EVA molecules are intercalated in the silicate layer, the chain conformation of the NR/EVA molecules is not readily changed because of geometric constraints, and the interactions between the polymer and the surface of the silicate layers become stronger. The changes in the density of the packing of polymer chains results in the modification of the conformation and orientation of chain segments in the neighborhood of the inorganic surface.[18] Therefore, their dynamic behavior is different from that of the pure NR/EVA blend. The significant reduction of the intensity of the tan δ peak also indicates a strong adhesion between the polymer and silicate layers.[19]

Thermogravimetric analysis (TGA)

Figure 12 shows the degradation curves for NR, EVA, and an NR/EVA blend. NR shows only one degradation step, with the onset temperature corresponding to 350°C. EVA undergoes two degradation steps. The first decomposition step is due to the release of acetic acid and starts at 290°C, and the second degradation step involves the polyethylene backbone, starts at 390°C, and leads to complete polymer volatilization. The NR/EVA blend also shows two degradation steps. The first is due to the NR phase, but the corresponding onset temperature is higher than that observed for pure NR. This behavior suggests the presence of EVA increases the thermal stability of pure

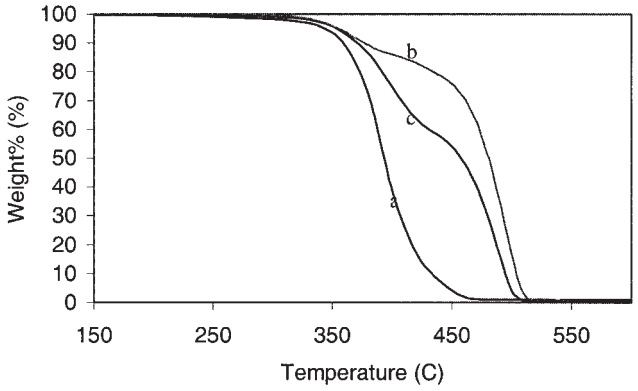

Figure 12 Thermograms of (a) NR, (b) EVA, and (c) the NR/EVA blend.

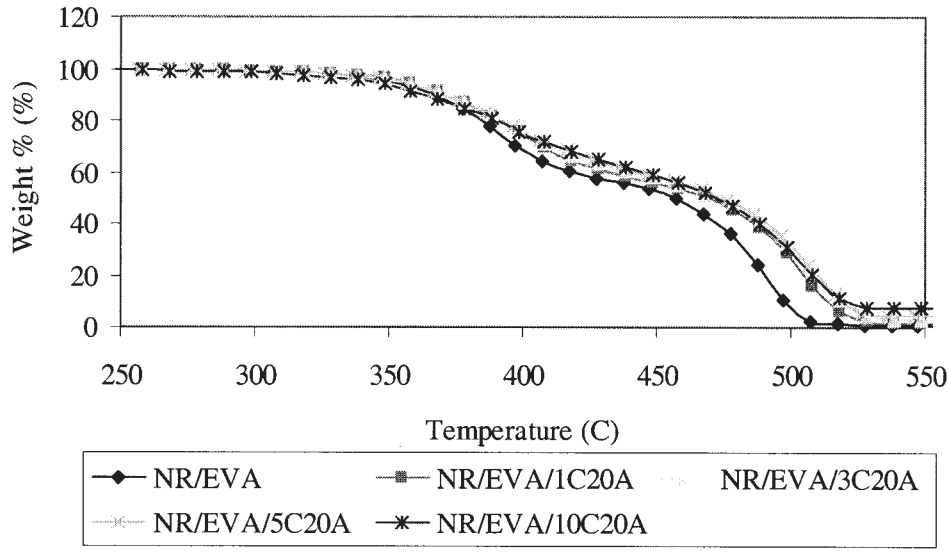

Figure 13 TGA results of NR/EVA/C20A nanocomposites.

NR. In addition, no degradation related to the acetate groups of EVA has been observed, and this indicates that EVA is also stabilized via blending with NR, as reported by Jansen and Soares.[20]

The effect of the organoclay on the degradation steps of the NR/EVA blends is presented in Figures 13 and 14. The presence of a layered silicate of C20A in this blend causes the degradation temperature of the blend to shift toward a higher temperature. The thermal stability improves with an increase in the organoclay content from 3 to 5 phr. A further increase in the C20A content (10 phr) does not improve the thermal stability of the blends anymore. Therefore, in this case, the optimal thermal stabilization is obtained at a filler content of approximately 5 phr. This result is similar to the findings reported by Alexandre et al.[21] Adding the organoclay delays the decomposition of the NR/EVA blend through the formation of char. At a very low clay content, no thermal stabilization can be observed, whereas increasing the amount of the nanofiller too much also decreases the thermal stability. Such behavior could account for the change in the relative proportions of exfoliated and intercalated species with the filler content. At low filler contents, exfoliation dominates, but the concentration of exfoliated particles is not high enough to promote thermal stability through char formation.[21] When the filler content is high, relatively more exfoliated particles are formed, and so char forms more easily and increases the thermal stability of the nanocomposites until a

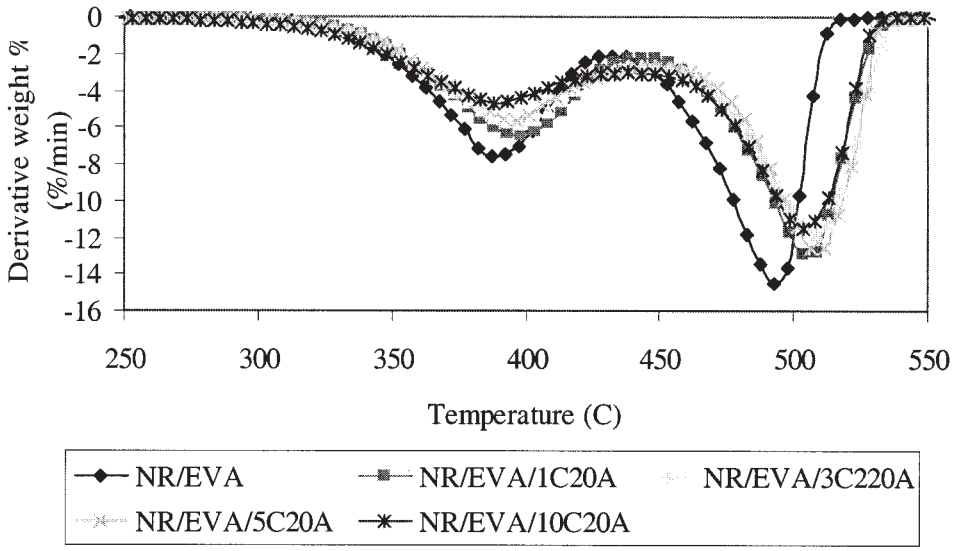

Figure 14 Differential thermogravimetry results of NR/EVA/clay nanocomposites.

nanofiller concentration of 5 phr is reached. At higher levels (10 phr), equilibrium between exfoliation and intercalation is drawn toward intercalation, and even if char is still formed in a high quantity, the morphology of the nanocomposites does not allow for maintaining good thermal stability.

CONCLUSIONS

The preparation of NR/EVA (60/40)-blend-based nanocomposites with the organoclay C20A and DDA-MMT was successfully carried out via melt blending with an internal mixer. The organoclay was partly exfoliated, as revealed by TEM pictures, partly intercalated on the basis of XRD and TEM, and partly aggregated, as shown by SEM micrographs. The tensile modulus at 300% elongation of the nanocomposites was higher than that of the unfilled blend because of the increase in the stiffness of the polymer matrix. The tensile strength of the NR/EVA/DDA-MMT nanocomposites was better than that of NR/EVA/C20A. The poor strength of the nanocomposites was also contributed by the incompatibility effect of NR and EVA. The elastic modulus increased with increasing C20A and DDA-MMT content from −140 to 200°C. T_g increased systematically because of the reinforcement effect of silicate layers. The thermal properties of the blends also improved with the incorporation of the organoclay, as revealed by the TGA results.

The authors thank Rafi and Ho Oi Kuan from the Microscopy and Microanalysis Unit of Universiti Putra Malaysia for assisting them with obtaining transmission electron microscopy images. They are also grateful to Saiful and Zaiton Selamat from the Malaysian Institute for Nuclear Technology Research for helping them with obtaining scanning electron microscopy images. One of the authors (J.S.) is grateful to the Public Service Department of Malaysia for granting her a study leave.

References

1. Fu, X.; Qutubuddin, S. Polymer 2001, 42, 807.
2. Krishnamoorti, R.; Vaia, R. A.; Giannelis, E. P. Chem Mater 1996, 9, 1728.
3. Kato, M.; Usuki, A.; Okada, A. J Appl Polym Sci 1997, 66, 1781.
4. Vaia, R. A.; Ishii, H.; Giannelis, E. P. Chem Mater 1993, 5, 1694.
5. Alexander, M.; Dubois, P. Mater Sci Eng R 2000, 28, 1.
6. Zanetti, M.; Camino, G.; Thomnn, R.; Mulhaupt, R. Polymer 2001, 42, 4501.
7. Zanetti, M.; Kashiwagi, T.; Falqui, L.; Camiro, G. Chem Mater 2002, 14, 881.
8. Vu, Y. T.; Mark, J. E.; Pham, L. H.; Engelhardt, M. J Appl Polym Sci 2001, 82, 1391.
9. Arroyo, M.; Lopez-Machado, M. A.; Herrero, B. Polymer 2003, 44, 2447.
10. Chow, W. S.; Mohd Ishak, Z. A.; Karger-Kocsis, J.; Apostolov, A. A.; Ishiaku, U. S. Polymer 2003, 44, 7427.
11. Koshy, A. T.; Kuriakose, B.; Thomas, S.; Premalatha, C. K.; Varghese, S. J Appl Polym Sci 1993, 49, 901.
12. Koshy, A. T.; Kuriakose, B.; Thomas, S. Polym Degrad Stab 1992, 36, 137.
13. Tabtiang, A.; Lumlong, S.; Venables, R. A. Eur Polym J 2000, 36, 2559.
14. Kojima, Y.; Usuki, A.; Kawasumi, M.; Okada, A.; Kurauchi, T.; Kamigaito, O. J Polym Sci Part A: Polym Chem 1993, 31, 1755.
15. Uhl, F. W.; Davuluri, S. P.; Wong, S. C.; Webster, D. C. Polymer 2004, 45, 6157.
16. Noh, M. W.; Lee, D. C. Polym Bull 1999, 42, 619.
17. Agag, T.; Koga, T.; Takeichi, T. Polymer 2001, 42, 3399.
18. Nielson, L. E. Mechanical Properties of Polymers and Composites; Marcel Dekker: New York, 1994, 2nd ed., 545.
19. Varghese, S.; Karger-Kocsis, J.; Gatos, K. G. Polymer 2003, 44, 3977.
20. Jansen, P.; Soares, B. G. Polym Degrad Stab 1996, 52, 95.
21. Alexandre, M.; Beyer, G.; Henrist, C.; Cloots, R.; Rulmont, A.; Jerome, R.; Dubois, P. Macromol Rapid Commun 2001, 22, 643.